

Quantized vortices in a rotating Bose-Einstein condensate with spatiotemporally modulated interaction

Deng-Shan Wang, Shu-Wei Song, Bo Xiong, and W. M. Liu

Beijing National Laboratory for Condensed Matter Physics, Institute of Physics, Chinese Academy of Sciences, Beijing 100190, China

(Received 16 March 2011; revised manuscript received 17 August 2011; published 11 November 2011)

We present theoretical analysis and numerical studies of the quantized vortices in a rotating Bose-Einstein condensate with spatiotemporally modulated interaction in harmonic and anharmonic potentials, respectively. The exact quantized vortex and giant vortex solutions are constructed explicitly by similarity transformation. Their stability behavior has been examined by numerical simulation, which shows that a new series of stable vortex states (defined by radial and angular quantum numbers) can be supported by the spatiotemporally modulated interaction in this system. We find that there exist stable quantized vortices with large topological charges in repulsive condensates with spatiotemporally modulated interaction. We also give an experimental protocol to observe these vortex states in future experiments.

DOI: [10.1103/PhysRevA.84.053607](https://doi.org/10.1103/PhysRevA.84.053607)

PACS number(s): 03.75.Lm, 47.32.-y, 05.30.Jp

I. INTRODUCTION

The investigation of rotating gases or liquids is a central issue in the theory of superfluidity [1–4] since rotation can lead to the formation of quantized vortices which order into a vortex array, in close analogy with the behavior of superfluid helium. Under conditions of rapid rotation, when the vortex density becomes large, atomic Bose gases offer the possibility to explore the physics of quantized vortices in novel parameter regimes. During recent years, there have been advances in experimental discoveries [5–7] of rotating ultracold atomic Bose gases, and these developments have been reviewed in [8].

Theoretical studies mainly make use of the mean-field Gross-Pitaevskii (GP) equation to describe the main features of the vortex states [9,10], and several predictions [10] have been shown to agree with experiments [11]. Some of the important studies were concerned with the equilibrium properties of a single vortex, including its structures and dynamics [10], the critical frequency, and the nonlinear dynamics of vortex lattice formation [12]. A multiquantum vortex is typically dynamically unstable in harmonically trapped BEC predicted by several theoretical studies [13–15]. The splitting instability in the case of multiquantum vortices shows that the vortex will split into single quantum vortices even in the absence of dissipation due to the peculiar feature of nonlinear dynamics [16,17]. However, in the presence of a plug potential [18] or an anharmonic trapping potential [19,20], various studies have addressed different means to stabilize multiquantum vortices in rotating BEC. For example, when the confining potential is steeper than harmonic potential in the plane perpendicular to the axis of rotation, multiquantum vortices are energetically favorable if the interaction is weak enough. For stronger interactions, the multiply quantized vortices break up into arrays of several vortices. In addition, interestingly, stable multiquantum vortices have also been found to exist in two-component BEC [21], which can be adjusted near Feshbach resonance through spatial inhomogeneous external magnetic field B [i.e., $B = B(x)$].

Mathematically, the GP equation, to be written explicitly, is an equation of nonlinear Schrödinger type [22–28]. This equation has been studied extensively both in the physical and mathematical literature, since they provide a universal

model for a study of the dynamics of the envelope waves. One of the distinctive features of the equation as it appears in BEC problems is the presence of an external trapping potential, which essentially affects the elementary excitation spectrum. Most properties of the BEC are significantly affected by the interatomic interaction, which can be characterized by the s -wave scattering length [29]. Recent experiments have demonstrated that both amplitude and sign of the scattering length can be modified by utilizing the Feshbach resonance [30–32]. This technique provides a very promising method for the manipulation of atomic matter waves and the nonlinear excitations in BEC by tuning the interatomic interaction. By using this technique, one can study atomic matter waves and the nonlinear excitations in BEC for the case of the GP equations with the time- and space-dependent nonlinearity coefficients [23–26]. More recently, Yamazaki *et al.* [32] demonstrated experimentally submicron spatial control of interatomic interactions in a BEC of ytterbium successfully by utilizing optical Feshbach resonance technique.

Motivated by stabilizing multiple vortex states and understanding the behavior of nonlinear excitation in physical systems, we perform theoretical analysis and numerical studies of the quantized vortices in a rotating BEC with spatiotemporally modulated interaction in harmonic and anharmonic potentials, respectively. Compared with the former work on quantized vortices, we find that a new series of exact single and multiple vortex states (defined by radial and angular quantum numbers) can be supported by the spatiotemporally modulated interaction in a rotating BEC. In particular, our results have provided a very promising method for stabilizing the vortex having very large topological charge $S \geq 2$, which has been conjectured unstable [33] by tuning the external potential and nonlinear interaction simultaneously in time.

II. THE THEORETICAL MODEL AND EXACT VORTEX SOLUTIONS

At zero temperature, the quantum and thermal fluctuations are negligible so that a BEC trapped in an external potential can be described by a “macroscopic wave function” $\Psi(\mathbf{r}, t)$ obeying the GP equation. In the rotating frame with rotating

frequency Ω_0 around the z axis, the GP equation in cylindrical coordinate reads

$$i\hbar \frac{\partial \Psi}{\partial t} = \left(-\frac{\hbar^2}{2m} \nabla^2 - \frac{\hbar^2}{2m} \frac{\partial^2}{\partial z^2} + V_{\text{ext}} + G|\Psi|^2 \right) \Psi + i\hbar \Omega_0 \frac{\partial \Psi}{\partial \theta},$$

where $\nabla^2 = \partial^2/\partial x^2 + \partial^2/\partial y^2 = \partial^2/\partial r^2 + 1/r \partial/\partial r + 1/r^2 \partial^2/\partial \theta^2$ with $r^2 = x^2 + y^2$, m is the atom mass, θ is the azimuthal angle, the wave function is normalized by the total particle number $N = \int d\mathbf{r} |\Psi|^2$, V_{ext} is an external trapping potential, and $G = 4\pi\hbar^2 a(r,t)/m$ represents the strength of interatomic interaction characterized by the s -wave scattering length $a(r,t)$, which can be adjusted experimentally by an inhomogeneous external magnetic field $B = B(x,y,t)$ in the vicinity of a Feshbach resonance [30,31]. The trapping potential can be assumed to be $V_{\text{ext}} = m(\omega_r^2 r^2 + \omega_z^2 z^2)/2$, where ω_r and ω_z are the confinement frequencies in the radial and axial directions, respectively, and in particular, the radial confinement frequency ω_r is assumed to be time dependent as in [25,34]. In the following, we consider the atoms in the $|F = 1, m_F = 1\rangle$ hyperfine state of ${}^7\text{Li}$ and $|F = 1, m_F = 1\rangle$ hyperfine state of ${}^{87}\text{Rb}$ trapped in a very thin disk-shaped potential [i.e., the trapping potential in the radial direction is much weaker than that in the axial direction as $\omega_r(t)/\omega_z \ll 1$], such that the motion of atoms in the z direction is essentially frozen to the ground state $\varphi(z)$ of the axial harmonic trapping potential.

Then we can separate the wave function as $\Psi(\mathbf{r},t) = \psi(x,y,t)\varphi(z)$ to derive the two-dimensional (2D) GP equation,

$$i\hbar \frac{\partial \psi}{\partial t} = -\frac{\hbar^2}{2m} \nabla^2 \psi + \frac{m}{2} \omega_r^2 r^2 \psi + G\eta |\psi|^2 \psi + i\hbar \Omega_0 \frac{\partial \psi}{\partial \theta}, \quad (1)$$

with $\eta = \int dz |\varphi(z)|^4 / \int dz |\varphi(z)|^2$. Introducing the scales characterizing the trapping potential, the length, time, and wave function are scaled as

$$x = a_h \tilde{x}, y = a_h \tilde{y}, t = \tilde{t}/\omega_z, \psi = \tilde{\psi}/a_h \sqrt{4\pi a_0 \eta},$$

respectively, with $a_h = (\hbar/m\omega_z)^{1/2}$ and a_0 is a constant length chosen to measure the s -wave scattering length. After the tilde is omitted, the 2D GP equation (1) is reduced to a dimensionless form as

$$i \frac{\partial \psi}{\partial t} = -\frac{1}{2} \nabla^2 \psi + V(r,t)\psi + g(r,t)|\psi|^2 \psi + i\Omega \frac{\partial \psi}{\partial \theta}, \quad (2)$$

where the interaction strength $g(r,t) = a(r,t)/a_0$, $\Omega = \Omega_0/\omega_z$ and the radial trapping potential can be written as $V(r,t) = \omega^2(t)r^2/2$ with $\omega(t) = \omega_r(t)/\omega_z$. In what follows, we consider not only the harmonic potential like this but also an anharmonic potential.

In order to find the exact vortex solutions to Eq. (2) with spatiotemporally modulated interaction, we first assume its exact solution as

$$\psi(r,\theta,t) = e^{iS\theta + i\phi(r,t)} \rho(r,t) U[R(r,t)], \quad (3)$$

where S is the topological charge related to the angular momentum of the condensate, $\rho(r,t)$ denotes the amplitude of wave function, and $R(r,t)$ is an intermediate variable reflecting the changes of the main wave function U . Substituting Eq. (3) into (2) and furthermore, letting $U[R(r,t)]$ satisfy

$$d^2 U/dR^2 + \mu_0 U + \mu_1 U^3 = 0, \quad (4)$$

where μ_0 and μ_1 are real constants, we can get a set of partial differential equations (PDEs) about $\rho(r,t)$, $R(r,t)$, $\phi(r,t)$, $V(r,t)$, and $g(r,t)$ as

$$\begin{aligned} R_t + \phi_r R_r &= 0, \\ 2g\rho^2 + \mu_1 R_r^2 &= 0, \\ \rho R_r + 2r\rho_r R_r + r\rho R_{rr} &= 0, \\ r\rho\phi_{rr} + 2r\phi_r \rho_r + \rho\phi_r + 2r\rho_t &= 0, \\ \frac{\rho_{rr}}{\rho} - 2\phi_t - \phi_r^2 - \frac{S^2}{r^2} + 2\Omega S + \frac{\rho_r}{\rho r} - 2V - \mu_0 R_r^2 &= 0, \end{aligned} \quad (5)$$

where subscripts r and t mean the derivative of function with respect to r and t . If letting $V(r,t) = \omega(t)^2 r^2/2 - \mu_0 R_r^2/2$ ($\mu_0 = 0$ corresponds to harmonic potential) and $\phi(r,t) = f_1 r^2 + f_2$ (f_1 and f_2 are time-dependent functions, and f_1 is frequency chirp and f_2 is phase), then solving the set of PDEs (5) we get

$$\rho(r,t) = e^{-2 \int f_1 dt} \Theta(r e^{-2 \int f_1 dt}), \quad (6)$$

and

$$R(r,t) = \int_0^{r e^{-2 \int f_1 dt}} 1/[\Theta^2(\tau)\tau] d\tau, \quad (7)$$

and

$$g(r,t) = -\mu_1 R_r^2/2\rho^2, \quad (8)$$

where μ_1 is a parameter controlling the sign of interaction parameter $g(r,t)$, $\Theta(\tau)$ is defined by Whittaker M and W functions [35], that is, $\Theta(\tau) = [c_1 M(\lambda_1/4\lambda_2, S/2, \lambda_2 \tau^2) + c_2 W(\lambda_1/4\lambda_2, S/2, \lambda_2 \tau^2)]/\tau$, where $\lambda_1, \lambda_2, c_1, c_2$ are nonzero constants and $c_1 c_2 > 0$. In particular, the above f_1 and f_2 satisfy the following two ordinary differential equations:

$$\begin{aligned} 2\Omega S - \lambda_1 e^{-4 \int f_1 dt} - 2df_2/dt &= 0, \\ \omega^2(t) + 4f_1^2 + 2df_1/dt - \lambda_2^2 e^{-8 \int f_1 dt} &= 0. \end{aligned} \quad (9)$$

When the parameter $\mu_0 = 0$, the external potential is just harmonic form $V(r,t) = \omega^2(t)r^2/2$, and we get explicit solution of Eq. (4) as $U(R) = v_1 \text{cn}(v_1 R + v_0, \sqrt{2}/2)/\sqrt{\mu_1}$, where v_0 and v_1 are arbitrary constants and $\mu_1 > 0$. So the exact vortex solution to Eq. (2) is

$$\psi = \frac{v_1}{\sqrt{\mu_1}} \rho e^{i(S\theta + f_1 r^2 + f_2)} \text{cn}(v_1 R + v_0, \sqrt{2}/2), \quad (10)$$

where functions ρ and R are given above. Here cn and sn (below) are Jacobi elliptic functions. When imposing the boundary conditions for vortex solution as $\lim_{|r| \rightarrow 0} \psi(r,\theta,t) = \lim_{|r| \rightarrow \infty} \psi(r,\theta,t) = 0$, we can get $v_0 = K(\sqrt{2}/2)$, $v_1 = 2nK(\sqrt{2}/2)/R(+\infty, 0)$, where $K(s) = \int_0^{\pi/2} [1 - s^2 \sin^2 \tau]^{-1/2} d\tau$ is the first kind elliptic integral and n is a nonnegative integer. In this case, since μ_1 should be positive and thus the interaction strength $g(r,t)$ is negative corresponding to the condensates consisting of ${}^{85}\text{Rb}$ [36] or ${}^7\text{Li}$ atoms [37,38] experimentally. The structures of the interaction parameter $g(r,t)$ with respect to radial coordinate r and time t are demonstrated in Fig. 1. It is observed that the interaction parameter is inverse Gaussian in r and periodic in t .

When the parameter $\mu_0 \neq 0$, the external potential becomes $V(r,t) = \omega^2(t)r^2/2 - \mu_0 R_r^2/2$ (an anharmonic potential) as

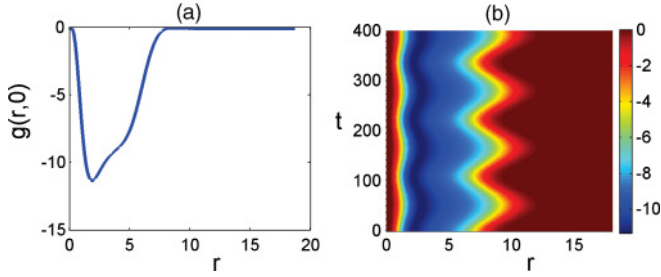


FIG. 1. (Color online) The spatiotemporally dependent interaction parameter $g(r,t)$ in Eq. (8) for parameter $\Omega = 0.7$, $\lambda_1 = 4$, $\lambda_2 = 2$, $c_1 = c_2 = 1$, $S = 1$, $\mu_1 = 1000$, and $\omega(t) = 0.028$. (a) The radial structure of $g(r,t)$ at $t = 0$. (b) The spatiotemporal structure of $g(r,t)$. Here the unit of length is $1.51 \mu\text{m}$ and the unit of time is 0.25 ms .

shown in Fig. 2, where there is a convex hull in the center of the harmonic potential, and the anharmonic potential is periodic in time t . We get the exact solution of Eq. (4) as $U(R) = \sqrt{2(\delta^2 - \mu_0)/\mu_1} \text{sn}(\delta R, \sqrt{\mu_0/\delta^2 - 1})$, where $\mu_0/2 < \delta^2 < \mu_0$ and $\mu_1 < 0$. So the exact vortex solution to Eq. (2) is

$$\psi = \sqrt{\frac{2(\delta^2 - \mu_0)}{\mu_1}} \rho e^{i(S\theta + f_1 r^2 + f_2)} \text{sn}(\delta R, \sqrt{\mu_0/\delta^2 - 1}), \quad (11)$$

where functions ρ and R are given above. When imposing the boundary conditions for vortex solution as $\lim_{|r| \rightarrow 0} \psi(r, \theta, t) = \lim_{|r| \rightarrow \infty} \psi(r, \theta, t) = 0$, we can get $\delta = 2nK(\sqrt{\mu_0/\delta^2 - 1})/R(\infty, 0)$. In this case, the parameter μ_1 should be negative and thus the interaction strength $g(r,t)$ is positive corresponding to the condensates consisting of ^{87}Rb [39] or ^{23}Na atoms [40] experimentally.

Seen from the exact vortex solutions (10) and (11), there exists two class of vortex states (distinguishing them with two quantum numbers which are radial node n and topological charge S , also called angular momentum quantum number) corresponding to the harmonic potential ($\mu_0 = 0$) and anharmonic potential ($\mu_0 \neq 0$) in attractive and repulsive BECs, respectively. In the following, we will first examine the

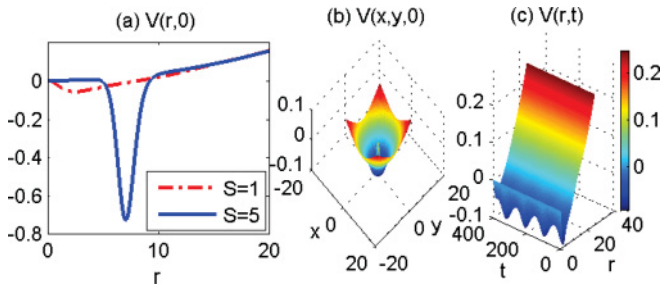


FIG. 2. (Color online) The shapes of the anharmonic potential $V(r,t) = \omega^2(t)r^2/2 - \mu_0 R_r^2/2$. (a) The radial structures of the anharmonic potential at $t = 0$ with parameters $S = 1$, $\delta = 7.4$ (dashed line), and $S = 5$, $\delta = 1172.4$ (solid line), respectively. (b) The spatial structure of the anharmonic potential at $t = 0$ with parameter $S = 1$, $\delta = 7.4$. (c) The spatiotemporal structure of the anharmonic potential with parameter $S = 1$, $\delta = 7.4$. The unit of time is 0.25 ms and the unit of length is $0.43 \mu\text{m}$ for the ^{87}Rb atom. The other parameters are $\Omega = 0.7$, $\lambda_1 = 4$, $\lambda_2 = 2$, $c_1 = c_2 = 1$, $\mu_0 = 62.2$, and $\omega(t) = 0.028$.

structures of these exact vortex solutions and then study the dynamic properties and stability of these vortex states under different situations.

III. STRUCTURES OF VORTEX STATES

The structures of the exact vortex solutions (10) and (11) can be controlled by modulating the frequency of the trapping potential and the spatiotemporal inhomogeneous s -wave scattering length as seen from Eq. (9). Taking into account the feasibility of the experiment, we only consider the case of harmonic potential ($\mu_0 = 0$) which corresponds to the attractive BEC as explained above.

In real experiment, we assume an attractive ^7Li condensate in the internal atomic state $|F = 1, m_F = 1\rangle$ [37,38] trapped in an axis-symmetric disk-shaped potential, where the axial confinement energy $\hbar\omega_z$ is much larger than the radial confinement and interaction energies, and the radial frequency of the trap is time dependent which can be written as

$$\omega(t) = \omega_r(t)/\omega_z = \omega_0 + \epsilon \cos(\omega_1 t), \quad (12)$$

with $0 \leq \epsilon < \omega_0$. For $\epsilon = 0$, the radial frequency of the trap is time independent and here, we choose the time-independent part of radial frequency $\omega_r = (2\pi) \times 18 \text{ Hz}$ and axial frequency $\omega_z = (2\pi) \times 628 \text{ Hz}$ as in [41], so $\omega(t) = \omega_0 = 0.028$.

As shown in Fig. 3, we demonstrate the density distributions for different radial quantum number n with fixed topological charge $S = 1$ at $t = 0$, which is based on the exact vortex solution (10). Figure 3(a) corresponding to $n = 1$ is a lowest

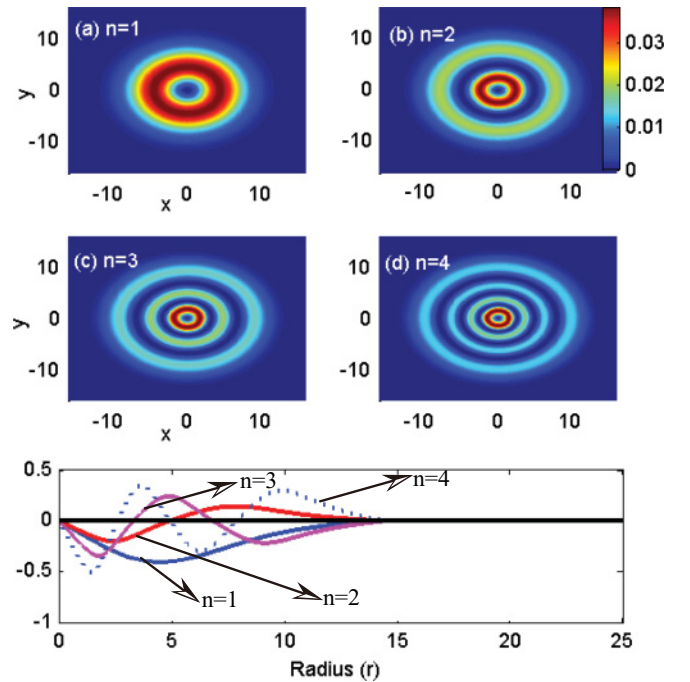


FIG. 3. (Color online) (a)–(d) The density distributions $|\psi(x,y,0)|^2$ (at $t = 0$), and the corresponding radial wave profiles (bottom) for the vortex solution (10) of the attractive rotating BEC for topological charge $S = 1$ and various radial quantum numbers. The parameters are $\Omega = 0.7$, $\mu_1 = 1000$, $\lambda_1 = 4$, $\lambda_2 = 2$, $c_1 = c_2 = 1$, $\epsilon = 0$, and $\omega_0 = 0.028$. Here the unit of length is $1.51 \mu\text{m}$ for ^7Li atom.

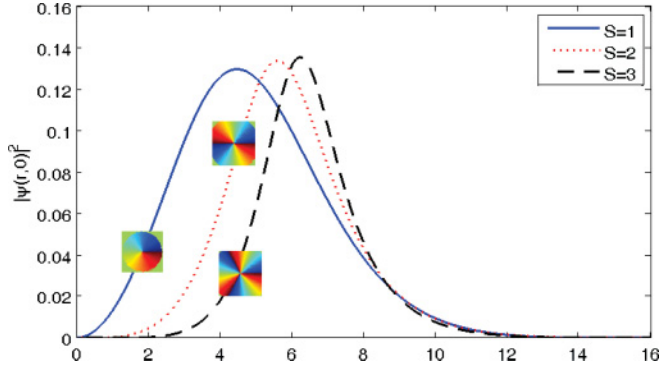


FIG. 4. (Color online) The radial structures of the density distributions and phase diagrams for the vortex solution (10) of the attractive rotating BEC with radial quantum number $n = 1$ and different topological charges at $t = 0$, where the unit of length is $1.51 \mu\text{m}$ for ^7Li atom. The insets are the corresponding phase diagrams and the other parameters are the same as Fig. 3.

energy state and Figs. 3(b)–3(d) corresponding to $n = 2, 3, 4$ are three excited states. In Fig. 3(e), we show the radial wave profiles of the exact vortex solution (10) at $t = 0$. It is clear to see that the number of ring structure of vortex solution increases by one with changing the radial quantum number n by one, which is similar to the quantum states of harmonic oscillator.

One of the interesting properties for the exact vortex solution (10) is shown in Fig. 4 by choosing different topological charge S with fixed radial quantum number $n = 1$. We can see that the density profiles of the vortex states become more and more localized with increasing the topological charge S due to the larger angular momentum for the higher topological charge S . Moreover, vortex expands outward with the increasing of the topological charges and so will obtain the larger angular momentum.

Another interesting aspect of the condensate is to study the monopole moment [34,42] defined by $\langle r \rangle = \int r |\psi|^2 dr$ which can be directly compared with experiments in BEC. In Fig. 5, we show the time evolution of the monopole moment for different oscillation frequencies ω_1 , amplitude ϵ in (12), and different radial quantum numbers $n = 1, 2$ with fixed topological charge $S = 1$. It is seen that the monopole moment represents regular oscillation following the oscillating frequency of the trap when ω_1 is large, but irregular oscillation when ω_1 is small which can be observed experimentally. The amplitude and center position of oscillation of monopole moment for the case $n = 2$ are a little larger than that for the case $n = 1$, but their periods are the same. In particular, at $\epsilon = 0$ (i.e., time-independent trapping potential), the oscillation of the monopole moment is only determined by the spatiotemporally nonlinear interaction which also represents regular behavior in our studied case. These phenomena connect to the resonance of certain collective modes in the system. It is seen that the interaction parameter $g(r, t)$ varies periodically in time from Fig. 1, and the frequency of the external potential can be modulated periodically as $\omega(t) = \omega_0 + \epsilon \cos(\omega_1 t)$. Therefore, the oscillating behavior of the monopole moment is the result of tuning interaction parameter and frequency of the external potential.

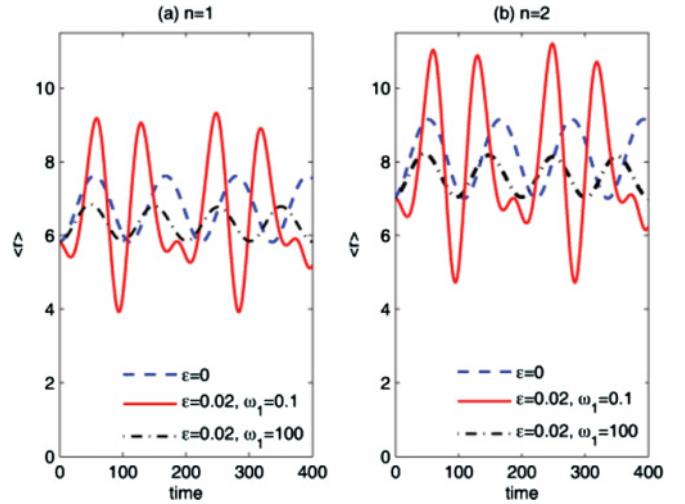


FIG. 5. (Color online) Time evolution of the monopole moment $\langle r \rangle$ in the attractive rotating BEC for different frequencies of the harmonic potential. (a) The radial quantum number is $n = 1$ and (b) $n = 2$. In both figures, the topological charge is $S = 1$, the frequency of the trap is $\omega(t) = \omega_0 + \epsilon \cos(\omega_1 t)$ with parameters $\Omega = 0.7$, $\omega_0 = 0.028$, $\lambda_1 = 4$, $\lambda_2 = 2$, $\mu_1 = 1000$, $c_1 = c_2 = 1$, and the unit of time is 0.25 ms.

IV. STABILITY ANALYSIS

It has been shown that attractive Bose condensates like ^{85}Rb and ^7Li become mechanically unstable and collectively collapse [30,31,38] when the number of atoms in the condensate exceeds critical value N_c . So it is important to produce the stable states in attractive Bose condensates. Saito and Ueda [34] have demonstrated that a matter-wave bright soliton can be stabilized in 2D free space by causing the strength of interactions to oscillate rapidly between repulsive and attractive by using, for example, Feshbach resonance [30,31]. In previous work, we [24] have found an exact stable localized nonlinear matter wave in quasi-2D BEC with spatially modulated nonlinearity in harmonic potential. In this section, we investigate the dynamical stability of the exact vortex solutions (10) and (11) by numerical simulation of Eq. (2). We show that only some types of the stable vortices (defined by radial and angular quantum numbers) can be supported by the spatiotemporally modulated interaction in this system.

In order to elucidate the dynamical stability of the exact vortex solutions proposed in Sec. II, we conduct numerical experiments by solving Eq. (2) and take the exact vortex solutions (10) and (11) at $t = 0$ as initial data. To begin with, we consider the attractive rotating BEC with harmonic potential at $\epsilon = 0$ in (12), which has exact vortex solution (10). In Fig. 6, we show the density evolutions and phase diagrams of the vortex solution (10) as the initial condition with radial quantum number $n = 1$ and different topological charge S or angular momentum quantum numbers based on numerical simulation of Eq. (2). It is shown that only when topological charge $S = 1$, vortex solution (10) is stable against perturbation with an initial Gaussian noise of level 0.5%, but for topological charge $S \geq 2$, giant vortex solution (10) will be

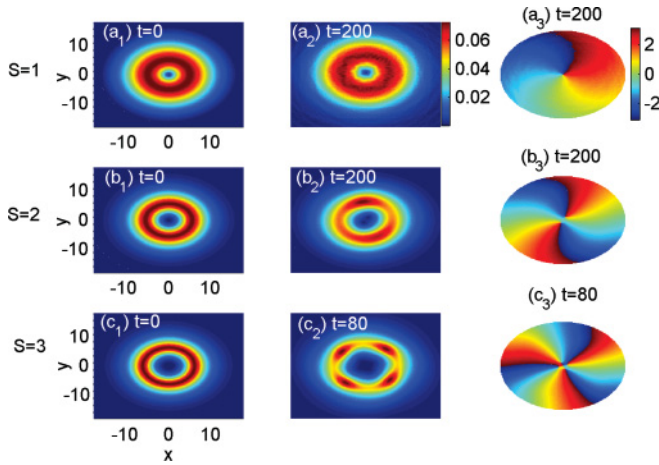


FIG. 6. (Color online) Time evolution of the density distributions $|\psi(x,y,0)|^2$ (at $t=0$) and phase diagrams for the vortex solution (10) of the attractive rotating BEC for radial quantum number $n=1$. (a) Stable vortex for topological charge $S=1$. (b) and (c) Unstable vortex for $S=2$ and 3, respectively. For all cases, the domain is $(x,y) \in [-15,15] \times [-15,15]$. The other parameters are $\Omega=0.7$, $\lambda_1=4$, $\lambda_2=2$, $\mu_1=1000$, $c_1=c_2=1$, $\epsilon=0$, and $\omega_0=0.028$. Here the unit of time is 0.25 ms and the unit of length is $1.51 \mu\text{m}$ for ^7Li atom.

unstable and split into single-charge vortices and so destruct the ring structures.

When the harmonic trap is time dependent which corresponds to $\epsilon \neq 0$ and $\omega_1 \neq 0$ in (12), Fig. 7 shows the unstable dynamics and phase diagrams of the giant vortex solution (10) with $S=3$ and two different radial quantum numbers $n=1,2$ for the attractive rotating BEC. It is observed that the time-dependent frequency of trap affects the dynamics of the vortex significantly. The instability of vortex states with $S=2$ and 3 in Figs. 6 and 7 is concerned with the resonance with the collective modes described by the harmonics with the angular momentum quantum number.

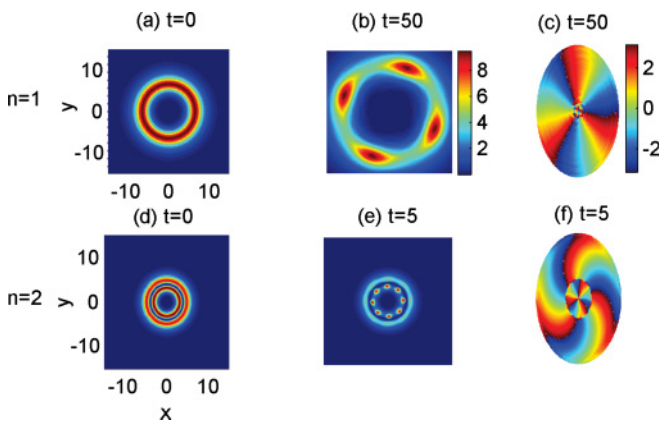


FIG. 7. (Color online) The dynamic instability of the vortex solution (10) of the attractive rotating BEC with time-dependent harmonic potential for topological charge $S=3$ and two different radial quantum numbers. Here the unit of time is 0.25 ms, the unit of length is $1.51 \mu\text{m}$ for ^7Li atom, and the parameters are $\Omega=0.7$, $\lambda_1=10$, $\lambda_2=5$, $\mu_1=1000$, $c_1=c_2=1$, $\omega_1=1$, $\epsilon=0.02$, and $\omega_0=0.028$.

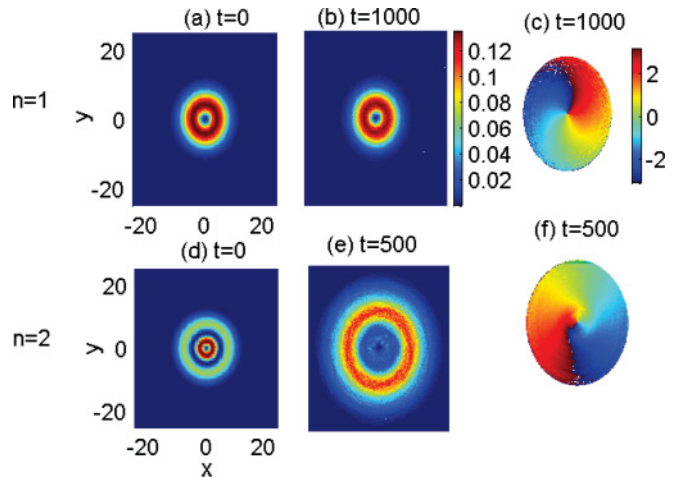


FIG. 8. (Color online) Time evolution of the density distributions $|\psi(x,y,0)|^2$ and phase diagrams for the vortex solution (11) of the repulsive rotating BEC for topological charge $S=1$ and radial quantum numbers $n=1$ and 2, respectively, with an initial Gaussian noise of level 0.5%. Here the domain is $(x,y) \in [-25,25] \times [-25,25]$, the parameters are $\delta=7.4$ (top) and $\delta=14.9$ (bottom), $\Omega=0.7$, $\lambda_1=4$, $\lambda_2=2$, $c_1=c_2=1$, $\mu_1=-10$, $\epsilon=0$, and $\omega_0=0.028$, the unit of time is 0.25 ms and the unit of length is $0.43 \mu\text{m}$ for ^{87}Rb atom.

Following the description in [3,43], we can explore the energy excitations near the stationary state by introducing a small deviation from the stationary state and linearizing the motion equation. Because the interaction parameter $g(r,t)$ and the frequency of the external potential vary following time, the vortex states may correspond to many high-energy collective excitation modes even for the lowest radial mode $n=1$. For the lowest mode with $n=1$ and angular momentum mode $S=1$, the vortex state is stable against a Gaussian noise. However, the vortex states with angular momentum modes $S=2$ and 3 in Figs. 6 and 7 are inclined to decay as they correspond to high-energy collective excitations. In addition, the vortex state with radial mode $n=2$ in Fig. 7 is also unstable as it corresponds to higher energy collective excitations.

Next we consider the repulsive rotating BEC in anharmonic potential $V(r,t) = \omega^2(t)r^2/2 - \mu_0 R_r^2/2$ with $\mu_0 \neq 0$ shown in Fig. 2, which has exact vortex solution (11). In Figs. 8 and 9, we demonstrate the density evolutions and phase diagrams of vortex solution (11) as the initial condition with different radial quantum numbers $n=1,2$ and fixed angular momentum quantum numbers $S=1$ and $S=5$, respectively. It is very interesting to note that when the radial quantum number $n=1$, the exact vortex solution (11) is always stable even for very large topological charge $S=5$, which is very different from the attractive rotating BEC with harmonic potential where a stable region for vortex solution (10) was found only for $S=1$ as shown in Fig. 6. Our results have provided a very promising method for stabilizing the giant vortex having very large topological charge $S \geq 2$ which has been conjectured unstable [33] by tuning the external potential and nonlinear interaction simultaneously in time. Numerical simulation shows that for the radial quantum number $n > 1$, the vortex solution (11) is always unstable for any topological charge S .

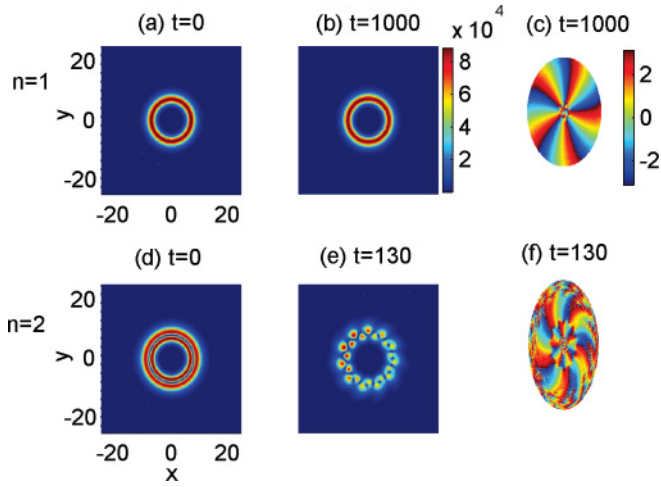


FIG. 9. (Color online) Time evolution of the density distributions $|\psi(x, y, 0)|^2$ and phase diagrams for the vortex solution (11) of the repulsive rotating BEC for topological charge $S = 5$ and radial quantum numbers $n = 1$ and 2 , respectively, with an initial Gaussian noise of level 0.5%. Here the domain is $(x, y) \in [-25, 25] \times [-25, 25]$, and the parameters are $\delta = 1172.4$ (top) and $\delta = 2344.9$ (bottom). The other parameters and units of time and length are the same as Fig. 8.

Finally, we investigate the effect of the slightly asymmetrical potential to the stability of quantized vortices. To do so, we take the asymmetrical external trap as $V(r, t) = \omega^2(t)[(1 + \epsilon_x)x^2 + (1 + \epsilon_y)y^2]/2 - \mu_0 R_r^2/2$, where parameters ϵ_x and ϵ_y describe small deviations of the trap from the axisymmetry. The ENS group [44] stirred a BEC of ^{87}Rb confined in this kind of magnetic trap using a focused laser beam. Figure 10

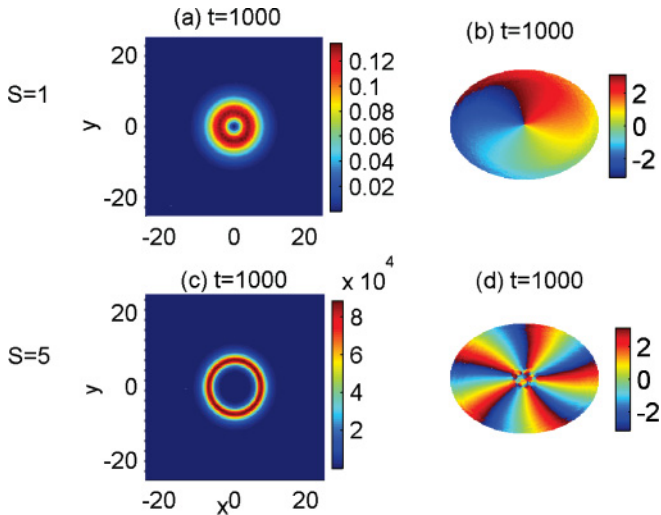


FIG. 10. (Color online) Density profiles and phase diagrams for the vortex solution (11) at $t = 1000$ for the repulsive inhomogeneous rotating BEC in slightly asymmetrical anharmonic potential $V(r, t) = \omega^2(t)[(1 + \epsilon_x)x^2 + (1 + \epsilon_y)y^2]/2 - \mu_0 R_r^2/2$ with $\epsilon_x = 0.02$ and $\epsilon_y = 0.03$. Here the quantum numbers $n = 1$ and topological charges $S = 1$ and 5 , respectively, and the level of the initial Gaussian noise is still 0.5%. The parameters are $\delta = 7.4$ (top) and $\delta = 1172.4$ (bottom). The other parameters are the same as Figs. 8 and 9. Here the unit of time is 0.25 ms and the unit of length is $0.43 \mu\text{m}$ for ^{87}Rb atom.

shows the evolutions of density profiles and phase diagrams of the vortex solution (11) at $t = 1000$ for the inhomogeneous repulsive rotating BEC in this slightly asymmetrical anharmonic potential with parameters $\epsilon_x = 0.02$ and $\epsilon_y = 0.03$. Here the quantum number $n = 1$ and topological charges $S = 1$ and 5 , respectively, and the level of the initial Gaussian noise is still 0.5%. It is seen that the quantized vortices with $S = 1$ and 5 in slightly asymmetrical anharmonic potential are still stable at $t = 1000$. The stability of these quantized vortices is related with collective modes described by the anharmonic potential, and the spatiotemporally modulated interaction and anharmonic potential can support stable giant vortex states.

We now give an experimental protocol to observe the above vortex states in future experiments. For the attractive interactions, we take ^7Li condensate in internal atomic state $|F = 1, m_F = 1\rangle$ [37,38], containing about 6.55×10^4 atoms, confined in a pancake-shaped trap with radial frequency $\omega_r = (2\pi) \times 18 \text{ Hz}$ and axial frequency $\omega_z = (2\pi) \times 628 \text{ Hz}$ [41]. Experimentally, this trap can be determined by a combination of spectroscopic observations, direct magnetic field measurement, and the observed spatial cylindrical symmetry of the trapped atom cloud [45]. For the repulsive interactions, we take ^{87}Rb condensate in internal atomic state $|F = 1, m_F = 1\rangle$ [39], containing about 8×10^5 atoms, confined in an anharmonic potential which is a pancake-shaped harmonic trap with radial frequency $\omega_r = (2\pi) \times 18 \text{ Hz}$ and axial frequency $\omega_z = (2\pi) \times 628 \text{ Hz}$ [41] plus a convex hull (see Fig. 2). The key step is how to realize the spatiotemporal variation of the scattering length. Near the Feshbach resonance [30,31], the scattering length $a_s(B)$ varies dispersively as a function of magnetic field B , that is, $a_s(B) = \tilde{a}[1 - \Delta/(B - B_0)]$, with \tilde{a} being the asymptotic value of the scattering length far from the resonance, B_0 being the resonant value of the magnetic field, and Δ being the width of the resonance at $B = B_0$. For the magnetic field in the z direction with gradient α along the x - y direction, we have $\vec{B} = [B_0 + \alpha B_1(x, y, t)]\vec{e}_z$. In this case, the scattering length is dependent on x, y and time t . So in real experiments, we can use the Feshbach resonance technique to realize spatiotemporal variation of the interaction parameters shown in Fig. 1. Finally, in order to observe the density distributions in Figs. 3 and 6–9 clearly in experiment, the atoms should be evaporatively cooled to low temperatures, say in the range of 50–150 nK.

V. CONCLUSIONS

In conclusion, we have investigated the quantized vortices in a rotating BEC with spatiotemporally modulated interaction in harmonic and anharmonic potentials, respectively. Two families of exact vortex solutions for the 2D GP equation are constructed explicitly by similarity transformation. It is interesting to see that a new series of stable giant vortex states with topological charge $S \geq 2$ can be supported by tuning the external potential and the spatiotemporally modulated interaction in this system. We hope that this paper will stimulate further research on quantized vortices and help to understand the behavior of nonlinear excitation in physical systems with spatiotemporally modulated interaction.

ACKNOWLEDGMENTS

This work was supported by National Natural Science Foundation of China (NSFC) under Grants No. 10934010 and No. 60978019, the National Key Basic Research Special Foundation of China under Grants No.

2009CB930701, No. 2010CB922904, No. 2011CB921502, and No. 2012CB821300, and NSFC–Research Grants Council under Grants No. 11061160490 and No. 1386-N-HKU748/10. D. S. Wang was supported by NSFC under Grant No. 11001263 and China Postdoctoral Science Foundation.

- [1] R. J. Donnelly, *Quantized Vortices in Helium II* (Cambridge University Press, Cambridge, 1991).
- [2] A. S. Parkins and D. F. Walls, *Phys. Rep.* **303**, 1 (1998).
- [3] C. J. Pethick and H. Smith, *Bose-Einstein Condensataion in Dilute Gases* (Cambridge University Press, Cambridge, 2001).
- [4] N. R. Cooper, *Adv. Phys.* **57**, 539 (2008).
- [5] D. A. Butts and D. S. Rokhsar, *Nature (London)* **397**, 327 (1999).
- [6] P. Engels, I. Coddington, P. C. Haljan, V. Schweikhard, and E. A. Cornell, *Phys. Rev. Lett.* **90**, 170405 (2003).
- [7] V. Schweikhard, I. Coddington, P. Engels, V. P. Mogendorff, and E. A. Cornell, *Phys. Rev. Lett.* **92**, 040404 (2004).
- [8] P. G. Kevrekidis and D. J. Frantzeskakis, in *Emergent Nonlinear Phenomena in Bose-Einstein Condensates: Theory and Experiment*, edited by R. Carretero-Gonzalez (Springer, New York, 2007).
- [9] F. Dalfovo, S. Giorgini, L. Pitaevskii, and S. Stringari, *Rev. Mod. Phys.* **71**, 463 (1999); D. L. Feder, A. A. Svidzinsky, A. L. Fetter, and C. W. Clark, *Phys. Rev. Lett.* **86**, 564 (2001).
- [10] J. J. Garcia-Ripoll and V. M. Perez-Garcia, *Phys. Rev. A* **64**, 053611 (2001); A. Aftalion and R. L. Jerrard, *ibid.* **66**, 023611 (2002); H. Saito and M. Ueda, *Phys. Rev. Lett.* **93**, 220402 (2004).
- [11] P. Rosenbusch, V. Bretin, and J. Dalibard, *Phys. Rev. Lett.* **89**, 200403 (2002).
- [12] A. A. Penckwitt, R. J. Ballagh, and C. W. Gardiner, *Phys. Rev. Lett.* **89**, 260402 (2002).
- [13] H. Pu, C. K. Law, J. H. Eberly, and N. P. Bigelow, *Phys. Rev. A* **59**, 1533 (1999); Y. Kawaguchi and T. Ohmi, *ibid.* **70**, 043610 (2004).
- [14] A. D. Jackson, G. M. Kavoulakis, and E. Lundh, *Phys. Rev. A* **72**, 053617 (2005); E. Lundh and H. M. Nilsen, *ibid.* **74**, 063620 (2006).
- [15] J. A. M. Huhtamäki, M. Möttönen, and S. M. M. Virtanen, *Phys. Rev. A* **74**, 063619 (2006).
- [16] T. Isoshima, M. Okano, H. Yasuda, K. Kasa, J. A. M. Huhtamaki, M. Kumakura, and Y. Takahashi, *Phys. Rev. Lett.* **99**, 200403 (2007).
- [17] H. M. Nilsen and E. Lundh, *Phys. Rev. A* **77**, 013604 (2008); P. Kuopanportti and M. Mottonen, *ibid.* **81**, 033627 (2010).
- [18] T. P. Simula, S. M. M. Virtanen, and M. M. Salomaa, *Phys. Rev. A* **65**, 033614 (2002).
- [19] E. Lundh, *Phys. Rev. A* **65**, 043604 (2002); C. Josserand, *Chaos* **14**, 875 (2004); A. D. Jackson, G. M. Kavoulakis, and E. Lundh, *Phys. Rev. A* **69**, 053619 (2004); H. Fu and E. Zaremba, *ibid.* **73**, 013614 (2006).
- [20] J. R. Abo-Shaer, C. Raman, J. M. Vogels, and W. Ketterle, *Science* **292**, 476 (2001).
- [21] J. Ruostekoski, *Phys. Rev. A* **70**, 041601(R) (2004).
- [22] C. Sulem and P. Sulem, *The Nonlinear Schrödinger Equation* (Springer-Verlag, Berlin, 1999).
- [23] J. Belmonte-Beitia, V. M. Perez-Garcia, V. Vekslerchik, and P. J. Torres, *Phys. Rev. Lett.* **98**, 064102 (2007); M. Salerno, V. V. Konotop, and Yu. V. Bludov, *ibid.* **101**, 030405 (2008).
- [24] D. S. Wang, X. H. Hu, J. Hu, and W. M. Liu, *Phys. Rev. A* **81**, 025604 (2010).
- [25] J. Belmonte-Beitia, V. M. Perez-Garcia, V. Vekslerchik, and V. V. Konotop, *Phys. Rev. Lett.* **100**, 164102 (2008); D. S. Wang, X. H. Hu, and W. M. Liu, *Phys. Rev. A* **82**, 023612 (2010).
- [26] L. Wu, L. Li, J. F. Zhang, D. Mihalache, B. A. Malomed, and W. M. Liu, *Phys. Rev. A* **81**, 061805(R) (2010).
- [27] Z. Yan and V. V. Konotop, *Phys. Rev. E* **80**, 036607 (2009); X. F. Zhang, X. H. Hu, D. S. Wang, X. X. Liu, and W. M. Liu, *Front. Phys.* **6**, 46 (2011).
- [28] K. Kasamatsu, M. Tsubota, and M. Ueda, *Phys. Rev. A* **66**, 053606 (2002).
- [29] E. Timmermans, P. Tommasini, M. Hussein, and A. Kerman, *Phys. Rep.* **315**, 199 (1999).
- [30] J. L. Roberts, N. R. Claussen, J. P. Burke, C. H. Greene, E. A. Cornell, and C. E. Wieman, *Phys. Rev. Lett.* **81**, 5109 (1998).
- [31] E. A. Donley, N. R. Claussen, S. L. Cornish, J. L. Roberts, E. A. Cornell, and C. E. Wieman, *Nature (London)* **412**, 295 (2001).
- [32] R. Yamazaki, S. Taie, S. Sugawa, and Y. Takahashi, *Phys. Rev. Lett.* **105**, 050405 (2010).
- [33] D. Mihalache, D. Mazilu, B. A. Malomed, and F. Lederer, *Phys. Rev. A* **73**, 043615 (2006); L. D. Carr and C. W. Clark, *Phys. Rev. Lett.* **97**, 010403 (2006).
- [34] H. Saito and M. Ueda, *Phys. Rev. Lett.* **90**, 040403 (2003).
- [35] M. Abramowitz and I. A. Stegun (editors), *Confluent Hypergeometric Functions* (Dover, New York, 1972).
- [36] S. L. Cornish, N. R. Claussen, J. L. Roberts, E. A. Cornell, and C. E. Wieman, *Phys. Rev. Lett.* **85**, 1795 (2000).
- [37] C. C. Bradley, C. A. Sackett, J. J. Tollett, and R. G. Hulet, *Phys. Rev. Lett.* **75**, 1687 (1995).
- [38] J. M. Gerton, D. Strekalov, I. Prodan, and R. G. Hulet, *Nature (London)* **408**, 692 (2000); S. E. Pollack, D. Dries, M. Junker, Y. P. Chen, T. A. Corcovilos, and R. G. Hulet, *Phys. Rev. Lett.* **102**, 090402 (2009).
- [39] M. H. Anderson, J. R. Ensher, M. R. Matthews, C. E. Wieman, and E. A. Cornell, *Science* **269**, 198 (1995); S. Burger, K. Bongs, S. Dettmer, W. Ertmer, K. Sengstock, A. Sanpera, G. V. Shlyapnikov, and M. Lewenstein, *Phys. Rev. Lett.* **83**, 5198 (1999).
- [40] A. J. Moerdijk, B. J. Verhaar, and A. Axelsson, *Phys. Rev. A* **51**, 4852 (1995).
- [41] G. Theocharis, D. J. Frantzeskakis, P. G. Kevrekidis, B. A. Malomed, and Y. S. Kivshar, *Phys. Rev. Lett.* **90**, 120403 (2003).
- [42] H. Saito and M. Ueda, *Phys. Rev. A* **70**, 053610 (2004); C. N. Liu, T. Morishita, and S. Watanabe, *ibid.* **75**, 023604 (2007).
- [43] S. Stringari, *Phys. Rev. Lett.* **77**, 2360 (1996).
- [44] K. W. Madison, F. Chevy, W. Wohlleben, and J. Dalibard, *Phys. Rev. Lett.* **84**, 806 (2000).
- [45] D. Rychtarik, B. Engeser, H. C. Nagerl, and R. Grimm, *Phys. Rev. Lett.* **92**, 173003 (2004).